Trapped-flux magnets characterization for application in synchronous machines

V Climente-Alarcon[1], A Smara[1], N Mineev[1,2], L Tomkow[1], B A Glowacki[1, 3, 4] and T Reis[5]

[1] Department of Materials Science and Metallurgy, University of Cambridge, Cambridge CB3 0FS, UK

[2] Bruker BioSpin AG, Industriestrasse 26, Faellanden 8117, Switzerland

[3] Institute of Power Engineering, Warsaw 02-981, Poland

[4] Epoch Wires Ltd. Cambridge CB22 6SA, UK

[5] Oswald Elektromotoren GmbH, Miltenberg 63897, Germany

E-mail: vc363@cam.ac.uk

Abstract. Trapped-flux magnets comprising stacked superconducting tape constitute a promising development to increase the power density of electrical machines, whilst at the same time keeping the complexity required in their construction in manageable levels that allow their use in applications such as aircraft propulsion.
However, the conditions in which superconducting stacks operate inside an electrical motor differ quite significantly from the materials characterization experiments commonly developed to model their behaviour. This work presents the results of studying the applicability of these devices as magnetic flux source in the rotor of synchronous machines considering the influence of whole magnetic circuit. Several aspects are assessed, such as flux harmonics, magnetization, losses and demagnetization. Analytical expressions, which provide limited accuracy but allow fast calculations, are used for this purpose. The results illustrate the different trade-offs that arise during the design of a synchronous electric motor using trapped-flux magnets.

1. Introduction

Trapped-flux magnets may offer a reasonable solution for the introduction of superconducting technology in rotating electrical machines. Either grown from a seed in a bulk form [1] or built by pilling up layers of superconducting tape [2], they act as stand-alone elements, providing once magnetized a source of magnetic flux density for the operation of the device, similarly to permanent magnets, with no need of further equipment, such as current leads, that increases the complexity of the machine's construction [3].

These suitable characteristics encouraged several recent works aimed at studying their applicability. In [4] bulks were proposed for a synchronous motor, though stacks of superconducting tape were preferred in [5] to build a linear motor. This approach is shared with [6] dedicated to aircraft propulsion applications, motivated by stack's superior mechanical characteristics compared to bulks [2,7], roughly similar to the substrate on which the superconducting layer is grown in addition to their easy

manufacturability, with reproducible characteristics, and the fact that any point defect is smoothed out by the stack's multilayered configuration.

Nevertheless, the advantages of using trapped-flux magnets come at the expense of an increased operational complexity. First, before operation the currents that produce the flux must be induced. The most immediate solution not adding further electrical circuits in the machine, is to use the stator winding itself for this purpose. Tooth-coil designs constitute a straightforward configuration for the stator winding of a fully superconducting machine, since it can be built by means of racetrack coils, which are bended just in one direction [8]. This allows magnetizing each pole in succession, provided the shaft, also equipped with cooling devices and thermal insulation, can withstand the corresponding mechanical forces caused by the unevenly magnetized poles. Distributed windings, on the other hand, feature a more complicate coil arrangement [9], however they can be fed with such a current configuration that magnetic flux is circulated at the same time following the center of each pole, the direct or *d*-axis, in order to magnetize all trapped-flux magnets in just one step. Either field cooling or zero field cooling procedures are possible for both stator winding types, depending on, among other things, the heat-removal system (if they are different for stator and rotor or common to both) and the materials used in the stator winding: normal conductors or superconductors. Normal conductors can be pulsed, whereas this procedure seems more difficult to be applied using a superconducting winding [10].

Once magnetized, the trapped flux must be kept undisturbed during the operation stage of the machine. Contrary to permanent magnets, the circulating currents in trapped-flux ones are macroscopic, and thus can be influenced by any variation of the magnetic flux density. Normal variations to the surface of the stack cause losses and heating [11], whereas tangential ones (cross-fields) alter the induced current's circulation pattern in such a way that effectively demagnetize the superconductor [12]. Unfortunately, such variations are intrinsic to the air-gap of an electrical machine, even when stator teeth are removed, due to the discrete layout of the stator coils.

Facing these complexities, the aim of this work is to provide an insight into the conditions in which trapped-flux magnets would operate inside an electrical machine. In this way the gap between laboratory testing and preliminary machine design can be bridged. Several aspects are treated: harmonic content of the magnetic flux density profile in surface mounted superconducting magnets in Section 2, flux leakage for interior mounted ones in Section 3, and the current linkage harmonics created by the stator, which cause demagnetization and losses, in Section 4. In all cases, despite their limited accuracy, analytical expressions are used, as it should be done during the first step of any design procedure. Finite element analysis is only utilized for validation purposes. Nevertheless, this limited approach well reproduces some characteristic behavior of trapped-flux magnets installed inside an electrical machine and allows to draw some conclusions in Section 5.

2. Harmonic content of the magnetic flux density waveform

In a first approximation, the electromagnetic torque T_e produced by a surface mounted permanent magnet synchronous machine can be written for sinusoidal quantities as:

$$T_e = -\frac{3}{2}\frac{p}{\omega}\frac{\hat{u}_s\hat{u}_p}{X_s} sin\ \delta \tag{1}$$

where p is the number of pole pairs, ω is the rotational speed in radians, X_s is the synchronous reactance, $\hat{u}_s$ the peak supply voltage, $\hat{u}_p$ the peak back-electromotive force and δ the load angle. In turn the back-emf $\hat{u}_p$ is directly proportional to the variation of the flux linkage created by the permanent magnets' movement in the air-gap. This means that it depends on the rotation speed and the peak value of the magnetic flux density wave main component $\hat{B}_p$, obtained from the Fourier series as it first coefficient:

$$\hat{B}_p = \frac{1}{\pi}\int_0^{2\pi} B_r(\varphi)\sin\varphi\, d\varphi\ . \tag{2}$$

In equation (2) $B_r(\varphi)$ is the profile of the magnetic flux density along the air-gap, usually a rectangular waveform for surface mounted permanent machines, and φ the electrical angle, which extends two pole pitches. The Fourier series coefficients b_k for rectangular, triangular and trapezoidal (with π/4 rise period) odd waveforms with amplitude unity (figure 1) can be written as:

$$b_{k\_rctn} = \frac{2}{\pi} \cdot \frac{1-(-1)^k}{k} \qquad b_{k\_trng} = \frac{4}{\pi^2} \cdot \frac{1-(-1)^k}{k^2} \qquad b_{k\_trpz} = \frac{4\sqrt{2}}{\pi^2} \cdot \frac{1-(-1)^k}{k^2} \qquad (3)$$

It is clear from (1-3) that a square wave, such as the one shown in figure 1 a), having a Fourier coefficient of b_{1_rctn}=4/π, theoretically maximizes the output torque in surface mounted permanent magnet motors. However, it must be said that in order to avoid cogging torque, consecutive permanent magnets are spaced along the rotor perimeter, yielding a rectangular magnetic flux density waveform with values of the Fourier coefficient slightly below 4/π.

On the other hand, trapped-flux magnets, if fully saturated, feature a triangular profile, whereas when undersaturated –not fully magnetized– the shape is rather trapezoidal [13]. This leads to the fact that a direct comparison between permanent and trapped-flux magnets taking into account its peak remanent magnetization is not correct for their application as surface mounted magnets in electrical machines. In order to yield the same torque, a fully saturated trapped-flux magnet must have a peak remanent flux 46% higher than permanent ones. That is, to surpass the actual state of the art value achieved by conventional means, 1.3 T, superconducting magnets will trap 1.9 T. This value is also the saturation level of silicon iron alloys employed in manufacturing the stator and rotor.

For lower levels of saturation, the trapezoidal profile of the magnetic flux density yields values of the Fourier series' b_k coefficients depending on the slope of the rising and descending segments, but always higher than for the triangular shape. This slope is related to J_c, the critical current or maximum current density the superconductor is able to carry, according to the Bean's model (see figure 2). Hence, in an electrical motor application, undersaturated high J_c trapped-flux magnets can yield higher values of torque compared to lower J_c fully saturated ones. This effect is illustrated in figure 1, b) and c) diagrams: a surface mounted trapped-flux magnet with double J_c will increase the torque 41% for the same peak level of magnetic flux density achieved during the magnetization process (1 T).

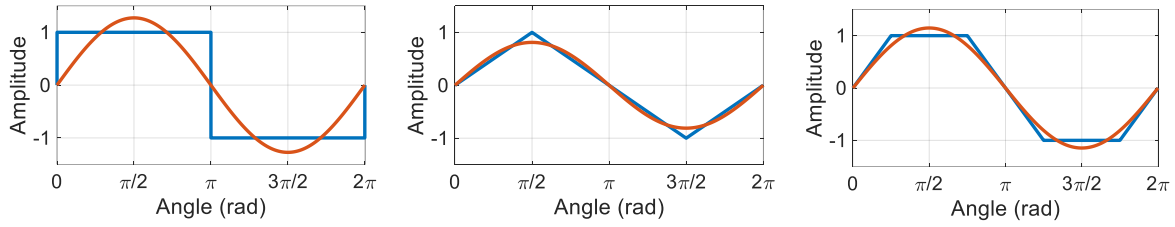

a) b) c)

Figure 1. Profile of different waveforms and their main sinusoidal component.

This analysis can be easily extended to higher order harmonics: superconducting magnets, compared to conventional ones, naturally portray lower amplitude high order harmonics (their order is squared in the denominator of (3) with k = 3,5,7…), which would lower the interactions with the stator current linkage harmonics in this surface mounted configuration, smoothing the output torque.

3. Leakage flux at the edges of the magnet

As said in the previous section, the profile of the magnetic flux density on the surface of trapped-flux magnets exhibit either a trapezoidal or a triangular shape. This is caused by the fact that this flux is generated by macroscopic currents distributed inside the superconductor following, in a first approximation, the Bean model. During magnetization, currents are induced below the sides' surface of

the superconducting magnet and, as the critical current level is reached there, flux is allowed to penetrate further into the superconductor, propagating these currents towards its centre. Figure 2 shows in a) the current density inside and in b) the corresponding magnetic field distribution over an unsaturated trapped-flux magnet of width $w_{stack} = 2a$. The limited magnetization process has left induced currents only at its sides, next to the surface of the material, penetrating up to depth x^*. The resulting trapezoidal magnetic field shape in figure 2 b), obtained simply by applying Ampere's law to the current density profile in figure 2 a), enhances a phenomenon shared with permanent magnets: leakage flux [14].

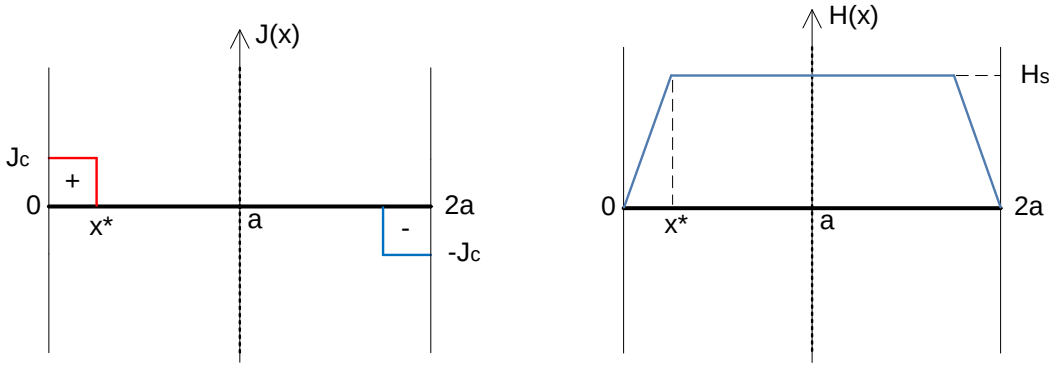

a) b)

Figure 2. Profiles of the current density, left, a); and magnetic field, right, b) inside an unsaturated trapped-flux magnet of width *2a*.

In electrical machines the linkage flux is the one common to two electrical circuits, whereas the leakage flux is the one that seeks alternative routes avoiding such commonality and thus it is usually wasted. Permanent magnets usually lose by these means 8-10% of their remanence despite being its relative magnetic permeability equal to one [15] and having a rectangular shape of the magnetic field on its surface. In the case of superconducting ones, the situation is not so favourable. In stacks the superconducting layer may be deposited on a substrate showing ferromagnetic behaviour at the temperature of operation [16], which on one hand favours magnetization, but on the other may increase the internal leakage flux inside the stack up to the point it is detrimental to the total field produced on its upper surface, as proved in [17]. In addition, ferromagnetic material surrounding the trapped-flux magnet, considered necessary in some designs in order to provide shielding against the air-gap harmonics and avoid demagnetization, facilitate leakage paths by providing low reluctivity between the central part of the magnet, with higher magnetic field, and its edges [figure 2 b)] [18].

For instance, figure. 3 shows a trapped-flux magnet made of pilled-up American Superconductor (AMSC) tape, with a critical current of 391 $A \cdot cm^{-1}$-width at 77 K and self-field and an engineering current density of $4.49 \cdot 10^8$ $A \cdot m^{-2}$. The magnet, surrounded by air, has been loaded by field cooling magnetization up to full saturation. As figure 3 illustrates, the magnetic flux density reaches a maximum value of 3.5 T at the center of the stack. In addition, leakage flux is also clearly appreciated as reverse flux along both sides of the magnet. This is not useful flux since it cannot be linked –it cannot flow– to other elements of the machine and, for instance, generate torque. The phenomenon worsens if ferromagnetic material is present at the top and bottom of the stack, due to the aforementioned reluctance reduction between the center and the edges of the magnet.

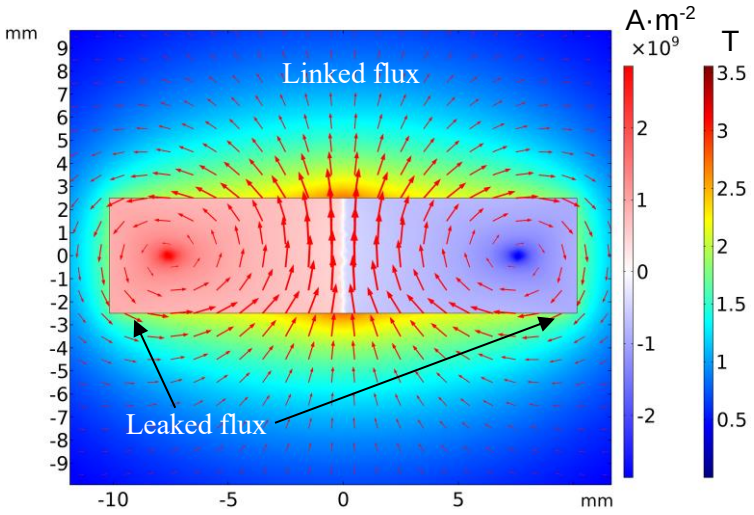

Figure 3. Circulation of magnetic flux density in and around a fully saturated stack (arrows). Leakage flux, returning along its sides, inside and outside the SC, is observed.

Thus, the aim of this section is to provide an analytical tool to obtain estimates about this leakage flux in a trapped-flux magnet installed inside an electrical machine, taking into account all the limitations this implies (air-gap between stator and rotor, limited magnetizing current and saturation of iron). For this purpose, a reluctance network, used to analyse simple magnetic circuits, is employed. It consists of modelling with lumped parameters the features present along the path of the magnetic flux circulation inside the machine and then applying the Hopkinson's law to obtain the common flux Φ:

$$\mathcal{F} = \Phi \cdot \mathcal{R} \,. \tag{4}$$

In equation (4) $\mathcal{F}$ accounts for the total magnetomotive force and $\mathcal{R}$ for the total reluctance, depending on geometric factors and permeability of the material.

The reluctance network is applied to a generic simplified geometry of a fully superconducting motor spanning two half poles or 36 deg [figure 4 b)]. This constitutes in the full cross-section of the machine the smallest unit into which it can be reduced, since during magnetization the flux is parallel to the centerline of the poles. The two trapped-flux magnets, having the same dimensions and composition as the one shown in figure 3, are installed inside the rotor iron, to protect them from the stator current linkage harmonics, moving in both directions along the air-gap. As in the novel rotor architecture developed for the ASuMED project's motor [18], the sides of the stacks are not covered by ferromagnetic material. This is intended to avoid further flux leakage and can be done for tape stacks under certain conditions due to the good mechanical properties of the substrate that assures structural stability. In addition, above the rotor, the stator portrays a teethless construction to suppress the stator slot harmonics caused by the variations in reluctance the teeth cause. The stator winding is installed in the air-gap and supported by a nonmagnetic structure, and hence not shown in figure 4. Other geometric and electrical characteristics of the model are shown in Table 1.

The reluctance network used to model the magnetization procedure is shown in figure 5 a). It reduces to lumped parameters calculated according to [19], each homogeneous area in the geometry of figure 4 along the central path of the flux. Each voltage source F_{coil} represent one of the two coils, fed with the same current, creating the magnetomotive force needed to induce the magnetic flux along the circuit. Two equal reluctances R_{airgap} model the air-gap at both sides of those coils. The two stacks are modelled similarly, as air-gaps with relative magnetic permeability equal to 1, by the parameter R_{stack}. The thinner stator yoke, shown in grey at the top of figure 4 saturates, and hence in the network [figure 5 a)] it is

reproduced as a variable reluctance whose value depends on the flux itself $R_{stator}(\Phi)$, yielding a non-linear problem that, however, can be solved in a few iterations. The rotor iron is not modelled due to its width, which yields a magnetic flux density well below saturation and thus a negligible value for its reluctance.

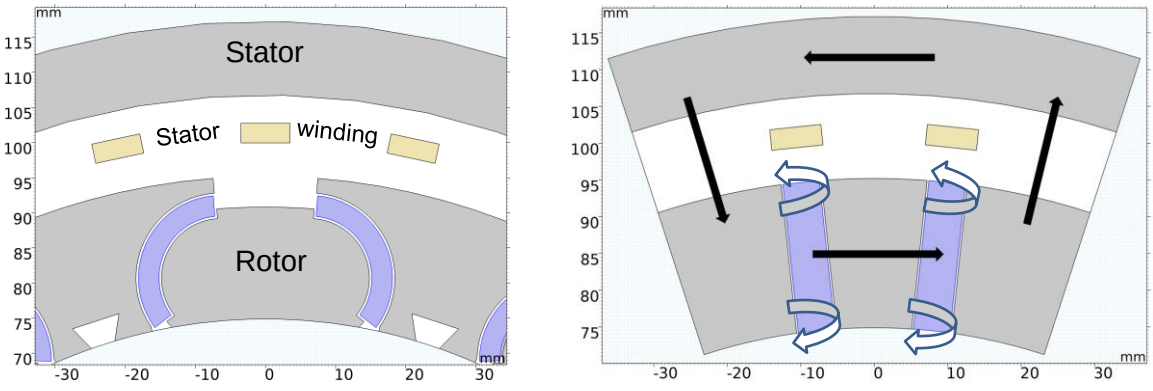

Figure 4. a) Rotor lay-out developed for the ASuMED motor and b) simplified section of the electrical machine studied in this work showing the central path of magnetic flux circulation during magnetization (black arrows) and leakage flux after magnetization (white arrows). Stacks are depicted in blue.

Table 1. Characteristics of the model.

Stator external diameter	236 mm
Stator internal diameter	214 mm
Stator winding distance to centre	101.5 mm
Stator coil cross section	2.8 x 7 mm
Air-gap length	12 mm
Stack length	5 mm
Rotor yoke external diameter	190 mm
Rotor yoke internal diameter	150 mm
Machine length	175 mm
Angle of the circular section	36 deg
Coil turns	6
Magnetizing current range	0.2 - 2.4 kA

In the first part of the study, the network in figure 5 a) is used to obtain the magnetic flux density circulating through all the elements of the circuit during magnetization, that is, when current is fed into the stator coils, in a range between 0.2 and 2.4 kA. After these magnetizing levels are reduced to 0, the reluctance network is modified as shown in figure 5 b). The superconducting magnets will maintain the same level of flux that was present during the magnetization procedure (thus the flux is trapped), hence in principle their magnetomotive force F_{stack} is equal to each one of the coils, F_{coil}, during magnetization. However, in order to fully model them, it must also take into account the leakage flux at both of their edges. This is done by adding a parallel branch [see the smaller loop in figure 5 b)], which aims at

reproducing both triangular regions at the sides of the trapezoidal shape shown in figure 2 b). As a first approximation, the magnetomotive force here is considered half of the one in the full magnet, $F_{leak}=F_{stack}/2$, whereas the new reluctances, R_{leak} and R_{stack}', are defined by the position of x^* in figure 2, that is the saturation of the magnet. This value of x^* is obtained according to the Bean model as:

$$x^* = \frac{w_{stack}}{2} \cdot \frac{\Phi_{induced}}{\Phi_{stack\_max}} \tag{5}$$

hence the position of x^* depends on the ratio between the flux crossing the superconducting magnet during field cooling magnetization $\Phi_{induced}$ and the maximum trapped flux for those dimensions, Φ_{stack_max}, obtained by FE simulation (see figure 3). The shift of x^* marking the critical current density penetration towards the centre is thus proportional to the saturation of the magnet and would reach the point *a* in figure 2 when it is fully saturated.

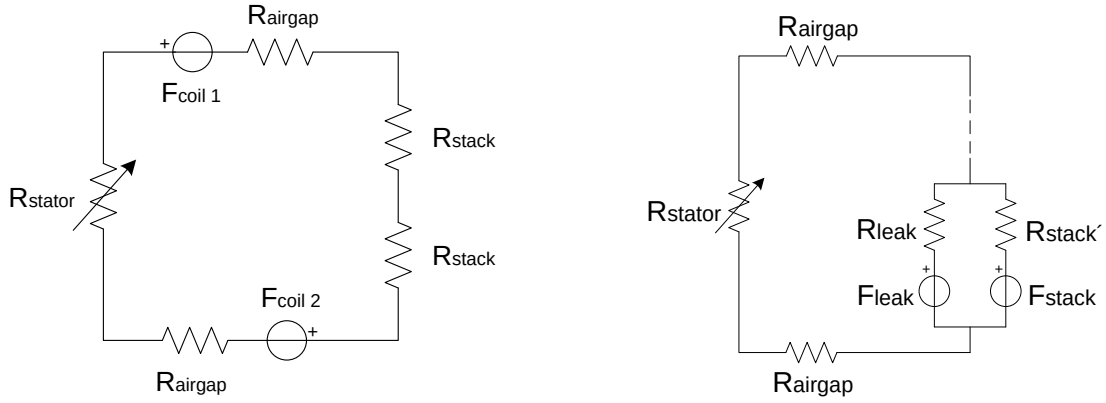

Figure 5. a) Proposed reluctance network to study the magnetization of the trapped-flux magnet and b) modification to the model after magnetization (only one stack's loop is depicted)

The accuracy of the network in figure 5 a) applied to the geometry of figure 4 b) is assessed by comparing its calculated induced flux during field cooling magnetization with the results of the field equations solved by the finite element (FE) method. In the FE case, the flux is measured at the surface facing the stack of the central rotor yoke piece's side. Figure 6 shows, that, although with similar shape, the error increases in the case of the reluctance network as the magnetizing current is raised, compared to FE. This stems from the fact the air-gap leakage flux is not modelled in the network and the performance of the reluctance network to reproduce the full distribution of magnetic flux in the saturated stator is limited.

The leakage flux at the edges of the trapped-flux magnet is shown at the bottom of figure 6 for both cases. In the FE model this leakage flux has been obtained by calculating the absolute value of the normal flux minus the actual normal flux on the rotor's iron yoke. This later is considered to be the linked or useful flux for torque production:

$$\Phi_{linked} = \Phi_{induced} - \Phi_{leakage} \,. \tag{6}$$

Conversely, the analytical model solution has been obtained from the reluctance network by applying Kirchhoff's voltage law to each loop and solving the corresponding system of equations iteratively for different levels of stator saturation until convergence is obtained. The results show that the method proposed here consistently underestimates the leaked flux, especially taking into account the higher values of induced flux during magnetization that the reluctance network yields (the difference between

the upper curves). This is caused by the fact that again not all the leakage paths are depicted in figure 5 b), especially the air region on top of the magnet, and that the superconducting region doesn't fulfill the Bean's model: increased leaked flux at the edges lowers J_c, pushing x^* in figure 2 towards the center of the stack [18] and thus allowing more leakage.

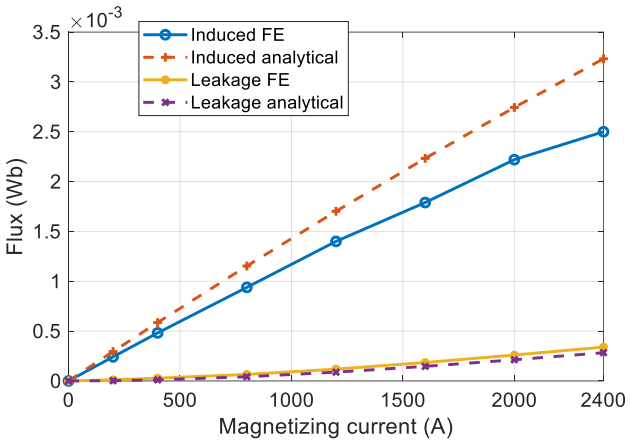

Figure 6. Comparison of flux values obtained by the reluctance network and by finite element analysis.

Nevertheless, the proposed approach suffices to qualitatively illustrate some characteristic behaviour of trapped-flux magnets arranged inside the rotor yoke of an electrical machine, that is, installed between ferromagnetic elements. Figure 7 shows the linked flux obtained using the proposed reluctance network for different total thicknesses (half millimetre of inert substrate + SC material thickness) of the stack and levels of magnetizing currents. As said, this linked flux, or useful flux, is equal to the induced flux during magnetization shown in figure 6 minus the leaked one. Each line represents one level of the magnetizing current fed to the coils, whose value is shown at the right-hand side of the diagram. The concave shape of the lines is determined by a trade-off: the higher magnetic reluctance of a thicker stack towards the right-hand side of the diagram limits magnetization for the same magnetizing current value, whereas the increased saturation of the stack to the left-hand side allows flux to leak at its sides, as x^* in figure 2 moves towards the centre of the stack. Thus, for each magnetizing current, there is a stack width identified with a square, where the useful trapped flux is maximized. No advantage is obtained either by reducing the thickness of the stack, to favour magnetization or by increasing it, to reduce the saturation and thus the leaked flux. Furthermore, this width is far greater than the one necessary to fully saturate the magnet: a 4 mm thick stack can trap an average magnetic flux density of 1.9 T, whereas here it is only loaded up to 1.13 T. This phenomenon, originated by the triangular/trapezoidal shape of the magnetic flux density provided by these elements compared to the rectangular one yielded by permanent magnets, imposes a heavy penalty for interior mounted stacks compared to surface mounted ones, since roughly twice the SC material amount is needed for suitable operation in the former case compared to the later.

Furthermore, the substitution of this extra SC material by inert –nonmagnetic– one yields little advantage, as it can be appreciated by the slopes at both sides of the maxima in figure 7. The remaining superconductor saturates faster than the reluctance provided, and the total leaked flux increases.

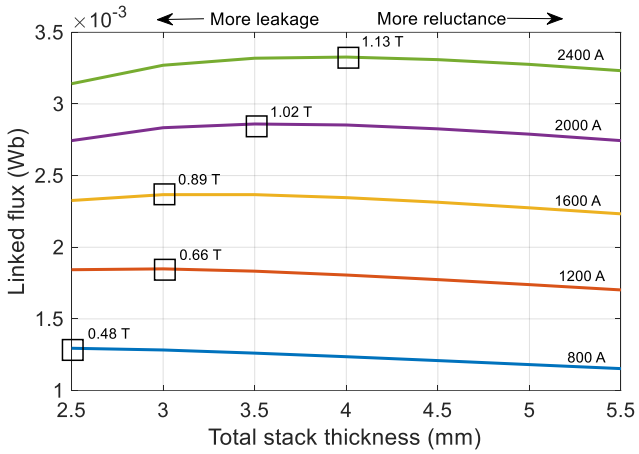

Figure 7. Comparison of linked flux values obtained by the reluctance network method for different stacks thickness and magnetizing current values

4. Losses and demagnetization

Variations in the magnetic flux density above a trapped-flux magnet cause losses, if those oscillations are normal to its surface, and demagnetization if they are tangential. In the air-gap of an electrical machine, the reluctance variation produced by the stator teeth as they move relative to the rotor, and the arrangement of the stator winding in discrete coils constitute the sources of those harmonics. Although the first can be removed in a teethless machine, as it is done in the design of figure 4, the stator winding, or also known as current linkage harmonics, will always be present in the air-gap. The value of these components can be estimated for losses computation [14] and in order to compare their amplitudes to the ones used during demagnetization experiments in laboratory conditions using simple analytical formulae [12]. For instance, with the configuration data of an electrical machine, the magnetomotive force $\widehat{\Theta}_{s\upsilon}$ for the harmonic of order υ can be written as [15]:

$$\widehat{\Theta}_{s\upsilon} = \frac{m \cdot k_{w\upsilon} \cdot N_s}{\pi \cdot p \cdot \upsilon} \hat{\imath}_s \tag{7}$$

where m is the number of phases, $k_{w\upsilon}$ the corresponding winding factor, N_s the number of series-connected turns in the stator, p the number of pole pairs and $\hat{\imath}_s$ the amplitude of the current fed into one phase, assumed sinusoidal. This creates on the surface of the rotor variations of magnetic flux density in the form:

$$\hat{B}_{s\upsilon} = \mu_0 \frac{\widehat{\Theta}_{s\upsilon}}{\delta_{ef}} \tag{8}$$

being μ_0 the magnetic permeability of vacuum and δ_{ef} the effective air-gap. For the machine of figure 4 this effective air-gap must consider besides the actual air-gap length, the reluctance of the iron, especially important when this material is closer to saturation. When utilizing (7-8) one must take into account that due to symmetries of an m-phase machine:

$$\upsilon = 1 \pm c \cdot 2 \cdot m, \quad c = 0,1,2 \ldots \tag{9}$$

The application of (7-9) to the design presented in figure 4 a) is shown in figure 8, for a current of 400 A_{rms}. An effective air-gap equivalent to twice the geometric one has been considered, and hence the saturation of the stator iron is not accounted. The figure shows that this simply obtained values are close

to the penetration field in a single stack's tape, and hence, an important level of demagnetization should be expected for a machine having this kind of superconducting magnets mounted on the surface of the rotor [12]. Furthermore, it can also be seen on the chart the effect on these harmonics of reducing the air-gap in 1 mm, which would favour magnetization, but also increases the possibility of demagnetization. Another trade-off arises in this case.

Furthermore, these stator winding induced components revolve around the rotor surface at frequencies:

$$\omega_{r\upsilon} = \omega_s \, (1 - \upsilon) \tag{10}$$

where ω_s is the synchronism speed. From (9) the first component $\upsilon = 1$ clearly moves at the same speed as the rotor. The frequencies for the higher harmonics ($\upsilon = 5\ldots,19$) lay between 0.4 and 2 kHz, which should be taken into account when carrying out experiments on demagnetization.

Finally, it is worth to mention that these stator harmonics will interact with the ones of the same order produced by the magnetic flux density profiles studied in Section 2, generating pulsating torques.

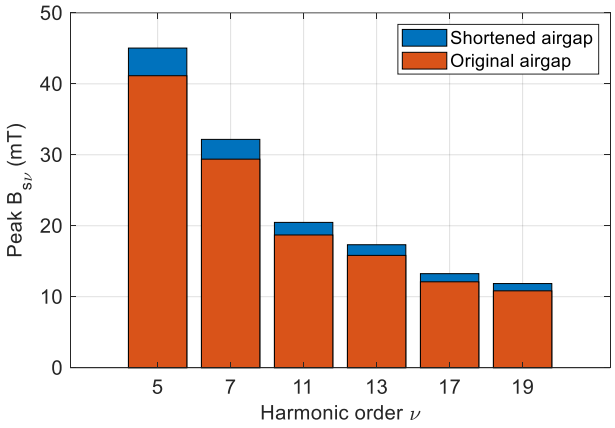

Figure 8. Effect in the stator induced harmonics of shortening 1 mm the airgap of the machine depicted in Fig. 4 b)

5. Conclusions

Analytical calculations constitute the first step in any design procedure. This contribution presents some approaches utilized in the electrical engineering's field, especially adapted here for the preliminary study of synchronous machine configurations having trapped-flux magnets as source of magnetic flux density. Although the accuracy of the procedures is limited when compared to finite element methods, they suffice to present some characteristic behaviour of superconducting magnets inside an electrical machine which may help to assess their applicability. In this line, the limitations of using interior mounted stacks have been portrayed, with the necessity of arranging, due to the leakage flux, twice the amount of the material needed for obtaining the same magnetic flux density when compared to surface mounted stacks. Furthermore, an approach to obtain an estimation on the variation of the magnetic flux density in the air-gap of a teethless electrical machine has been presented, along some remarks about the figures of merit necessary to compare trapped-flux magnets with conventional ones.

Acknowledgments

This research is financially supported by the European Union's Horizon 2020 research innovation programme under grant agreement No 723119 (ASuMED consortium) and EPSRC grant EP/P000738/1

References

[1] Durrell H, Dennis A R, Jaroszynski J, Ainslie M D, Palmer K G B, Shi Y-H, Campbell A M, Hull J, Strasik M, Hellstrom E E and Cardwell D A 2014 A trapped field of 17.6 T in melt-processed, bulk Gd-Ba-Cu-O reinforced with shrink-fit steel *Supercond. Sci. Technol.* **27** 082001.

[2] Patel A, Baskys A, Mitchell-Williams T, McCaul A, Coniglio W, Hänisch J, Lao M and Glowacki B A 2018 A trapped field of 17.7 T in a stack of high temperature superconducting tape *Supercond. Sci. Technol.* **31** 9.

[3] Song X, Bührer C et al. 2019 Designing and basic experimental validation of the world's first MW-class direct-drive superconducting wind turbine generator *IEEE Trans. Energy Conv.* (accepted for publication, DOI: 10.1109/TEC.2019.2927307).

[4] Durrell J H, Ainslie M D, Zhou D, Vanderbemden P, Bradshaw T, Speller S, Filipenko M and Cardwell D A 2018 Bulk superconductors: a roadmap to applications" *Supercond. Sci. Technol.* **31** 10 103501

[5] Sotelo G G, Sass F, Carrera M, Lopez-Lopez J and Granados X 2018 Proposal of a Novel Design for Linear Superconducting Motor Using 2G Tape Stacks *IEEE Trans. Ind. Elec*. **65** 9

[6] Climente-Alarcon V, Patel A, Baskys A and Glowacki B A 2019 Design considerations for electric motors using stacks of high temperature superconducting tape as permanent magnets *IOP Conf. Ser.: Mater. Sci. Eng.* **502** 012182.

[7] Li X, Li J, Zhou P, Liu K, Han L, Song X, Ma G, 2019, Decay of Trapped Magnetic Field in Stacks of YBCO Coated Conductors Subjected to Traveling Magnetic Waves *IEEE Trans. Appl. Supercond.* Vol. 29, No. 7, 520410.

[8] Jiang Y, Pei R, Hong Z, Jiang Q and Coombs T A, 2008, Design of an HTS motor *IOP J. Phys.: Conf. Ser.* **97** 012123.

[9] Wu D and Chen E 2011 Stator Design for a 1000 kW HTSC Motor With Air-gap Winding *IEEE Trans. Appl. Supercond.* **21** 3.

[10] Patel A, Baskys A, Hopkins S C, Kalitka V, Molodyk A and Glowacki B A 2015 Pulsed-Field Magnetization of Superconducting Tape Stacks for Motor Applications *IEEE Trans. Appl. Supercond.* **25** 3 5203405

[11] Rhyner J 1993 Magnetic properties and AC-losses of superconductors with power law current-voltage characteristics *Physica C* **212** pp. 292-300.

[12] Campbell A, Baghdadi M, Patel A, Zhou D, Huang K Y, Shi Y and Coombs T, 2017, Demagnetisation by crossed fields in superconductors *Supercond. Sci. Technol.*, **30** 3 034005

[13] Patel A, Hopkins S C, and Glowacki B A, 2013, Trapped fields up to 2 T in a 12 mm square stack of commercial superconducting tape using pulsed field magnetization *Supercond. Sci. Technol*, **26** 032001

[14] Iwasa Y 2009 *Case Studies in Superconducting Magnets, Design and Operational Issues* Second edition, (New York: Springer)

[15] Pyrhönen J, Jokinen T and Hrabovcová V 2014 *Design of Rotating Electrical Machines* Second edition, (New York: Wiley)

[16] Ijaduola A O, Thompson J R, Goyal A, Thieme C L H and Marken K, 2004, Magnetism and ferromagnetic loss in Ni–W textured substrates for coated conductors *Physica C* **403**, pp. 163-171.

[17] Baskys A, Patel A, Climente-Alarcon V and Glowacki B A 2019 Remanent Magnetic Flux Distribution in Superconducting-Ferromagnetic Layered Heterostructures, *Journal of Superconductivity and Novel Magnetism* (doi: 10.1007/s10948-019-5022-7).

[18] Climente-Alarcon V, Smara A, Patel A, Glowacki B, Baskys A. and Reis T, 2019, Field Cooling Magnetization and Losses of an Improved Architecture of Trapped-Field Superconducting Rotor for Aircraft Applications, *AIAA Propulsion and Energy Forum and Exposition,* Indianapolis, Indiana, USA, 19-22 August 2019, AIAA 2019-4313.

[19] Climente Alarcon V, Patel A, Baskys A and Glowacki B A 2019 Computation of Superconducting

Stacks Magnetization in an Electrical Machine, *IEEE Trans. Appl. Supercond.* (accepted for publication, doi: 10.1109/tasc.2019.2923537).

[20] Perho J, *Reluctance Network for Analysing Induction Machines* Edt. Helsinki University of Technology, Finland, 2002 (on-line: https://aaltodoc.aalto.fi/handle/123456789/2247)